Annals of Biomedical Engineering, Vol. 34, No. 4, April 2006 *(© 2006)* pp. 564–574
DOI: 10.1007/s10439-005-9071-7

Influence of Multiple Stenoses on Echo-Doppler Functional Diagnosis of Peripheral Arterial Disease: A Numerical and Experimental Study

CHRISTINE BERTOLOTTI,[1] ZHAO QIN,[2] BRIGITTE LAMONTAGNE,[1,2] LOUIS-GILLES DURAND,[1] GILLES SOULEZ,[3,4] and GUY CLOUTIER[2,4]

[1]Laboratory of Biomedical Engineering, Institut de Recherches Cliniques de Montréal, Montréal, Québec, Canada; [2]Laboratory of Biorheology and Medical Ultrasonics, Research Center, Centre hospitalier de l'Université de Montréal, Montréal, Québec, Canada; [3]Department of Interventional Radiology, Centre hospitalier de l'Université de Montréal, Montréal, Québec, Canada; and [4]Department of Radiology, Radio-Oncology and Nuclear Medicine, Université de Montréal, Montréal, Québec, Canada

(Received 4 August 2005; accepted 9 December 2005; published online: 9 February 2006)

Abstract—The objective of this paper was to evaluate the ability of the peak systolic velocity ratio (PSVR) and pressure drop (ΔP) to detect and grade multiple stenoses in lower limb mimicking arteries. Numerical simulations and experiments in vascular phantoms allowing ultrasound duplex scanning and pressure measurements were used to investigate simple and double stenotic arterial segments. Inter-stenotic distance, severity of the distal stenosis, flow rate and flow profile (steady or pulsatile) were the tested parameters. The three-dimensional simulations considered the turbulent two-equation Wilcox model. Agreements were observed between the experimental and numerical results for ΔP and PSVR. The maximum PSVR along the artery was shown to be mainly influenced by the severity of the most important stenosis. However, mutual interactions of both stenoses on hemodynamics were noted. By using the clinical PSVR threshold used to diagnose critical lesions (PSVR $\geq$ 2), its longitudinal evolution along the artery poorly reflected the length of the lesion or the impact of surrounding stenoses. This investigation confirms the interaction between adjacent stenoses on hemodynamics and its impact on the Doppler ultrasound index PSVR.

Keywords—Multiple arterial stenoses, Ultrasound diagnosis, *In vitro* experiments, Numerical simulations, Lower limb vascular diseases.

INTRODUCTION

Atheromatous infiltration in peripheral arterial disease (PAD) is usually diffuse, it is thus clinically important to localize the most hemodynamically significant stenosis to properly plan percutaneous or surgical revascularization, or lesions specifically suited to endovascular intervention.[7]

Address correspondence to Guy Cloutier, Eng., Ph.D., Director, Laboratory of Biorheology and Medical Ultrasonics, Research Center, University of Montreal Hospital, Pavilion J.A. de Sève (room Y-1619), 2099 Alexandre de Sève, Montréal, Québec, Canada, H2L 2W5. Dr. Cloutier is also Member of the Institute of Biomedical Engineering, Université de Montréal, Montréal, Québec, Canada. Electronic mail: guy.cloutier@umontreal.ca

Morphologic examination such as digital subtraction angiography (DSA), computed tomography angiography (CTA), and magnetic resonance angiography (MRA) cannot assess the hemodynamic significance of each individual lesion. Although Doppler ultrasound scanning measures flow velocities, hemodynamic disturbances induced by proximal stenoses can influence considerably the grading of distal obstructions, thus leading to a potential invalid diagnosis.

The pressure loss (ΔP), measured by the ankle/brachial systolic blood pressure ratio, is a non-invasive index representative of the global disease of lower limb vessels. The peak systolic velocity ratio (PSVR), measured with duplex ultrasound (US), allows the grading of individual stenoses non-invasively. Critical values of PSVR varying from 1.4 to 2.8 were proposed to detect lesions >75% in area reduction (50% in diameter reduction).[4,10,14,23,26] Nevertheless, most vascular centers use PSVR $\geq$ 2 as a well-established criterion for detecting hemodynamically significant stenoses.

The correlation between color Doppler guided ultrasound assessment of PSVR and DSA examination is approximately 80%, thus a mismanagement can occur in a high proportion of patients.[2,8,20,24] These discrepancies may be partially explained by the presence of multiple lesions, which are more difficult to grade. However, the influence of multiple stenoses on the clinical validity of PSVR is controversial. Several studies report no influence of adjacent disease on the correlation of PSVR with the angiographic diameter reduction.[14,24,28] Conversely, others report a lowering of sensitivity of Doppler ultrasound in the presence of multiple stenoses, especially for distal arteries of the lower limbs.[4,8,26]

Flow evaluation and modeling across single stenoses have extensively been investigated.[1,11,16,21,29,35,36,37] Available studies on flow modeling in multiple stenoses are mainly focusing on ΔP,[6,17,22,27,32] and some authors[27,32] do not agree on the non-linear hemodynamic additive

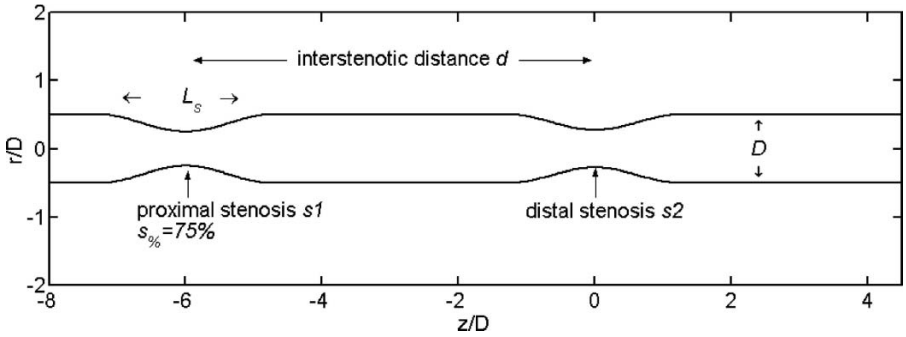

FIGURE 1. Geometry of double stenoses used for experimental and numerical models. *r* is the radial position, *z* is the longitudinal position, *D* is the diameter of the unobstructed section of the vessel, L_s is the length of each stenosis, and $s_{\%}$ is the stenosis severity in percentage of area reduction. The proximal stenosis is identified as *s1* and the distal obstruction as *s2* throughout this study.

effects of multiple stenoses. Moreover, numerical studies on modeled stenoses have been conducted under limiting assumptions such as: 2D axisymmetric and laminar flow conditions[6,17] or on vessels with a small diameter.[22] In this work, we propose to evaluate the influence of multiple stenoses on the PSVR threshold in a flow phantom and by numerical simulations.

MATERIALS AND METHODS

Computer simulations and *in vitro* experiments were performed on identical geometrical models, which include single or double stenoses of different severities separated by different inter-stenotic distances d (Fig. 1).

The stenosed vessel was represented as a straight cylinder including single or double stenoses of the same length $L_s = 20$ mm. The stenosis shapes were defined as cosine functions. If one considers $R = 3.95$ mm as being the radius of the unobstructed artery, $s_{\%}$ the stenosis severity in percent of cross-sectional area, z the longitudinal distance and r the radius of the stenosis, then the shape of each stenosis was given by:

$$r = R - e/2\,(1 - \cos 2\pi z/L_s)\,, \qquad \text{where} \qquad e = R\,(1 - \sqrt{1 - s_{\%}})\,. \tag{1}$$

In all modeled cases (see Table 1), the severity is expressed in term of area reductions (corresponding values of diameter reduction are presented in Table 2). The proximal stenosis *s1* had a fixed severity $s_{\%} = 75\%$, while the severity of the distal stenosis *s2* varied from moderate ($s_{\%} = 70\%$) to severe ($s_{\%} = 90\%$). The inter-stenotic distance d was 0 (single stenosis) or 3, 6, and 10 times the arterial diameter D of the unobstructed vessel for double stenoses.

Numerical Simulations

The Navier–Stokes equations that govern the mean flow were numerically solved with the finite element method using the Gambit and FIDAP packages (version 8.6, Fluent Inc, Lebanon, NH) on a Sparc, Solaris computer (4 GB RAM). Depending on the stenosis shape, the inflow mean Reynolds number $Re_m = \frac{4Q_m}{\pi D\nu}$ (where Q_m is the mean flow

Table 1. Experimental (×) and numerical (o) conditions tested in this study.

	s2 (%)		
	70	80	90
0, 196[a]	×, o	×, o	×, o
0, 392[a]	×	×	×
0, 588[a]	×	×	×
3*D*, 196[a]	×, o	×	×, o
3*D*, 392[a]	×	×	×
3*D*, 588[a]	×	×	×
6*D*, 196[a]	×, o		×, o
6*D*, 392[a]	×		×
6*D*, 588[a]	×		×
10*D*, 196[a]	o		o
6*D*, 212[b]	×		×

Note. The parameter *d* is the inter-stenotic distance, *D* is the diameter of the unobstructed artery, Re_m is the mean Reynolds number, *s2* is the severity in area reduction of the distal stenosis. For $d \neq 0$, the severity of the proximal stenosis *s1* was 75% in area reduction.
[a]Values of *d*, and Re_m.
[b]Values of *d*, and pulsatile Re_m.

Table 2. Correspondence table between stenosis severity defined in area reduction (left) or diameter reduction (right).

Area reduction *s* (%)	Diameter reduction *d* (%)
70	45
75	50
80	55
90	68
94	75

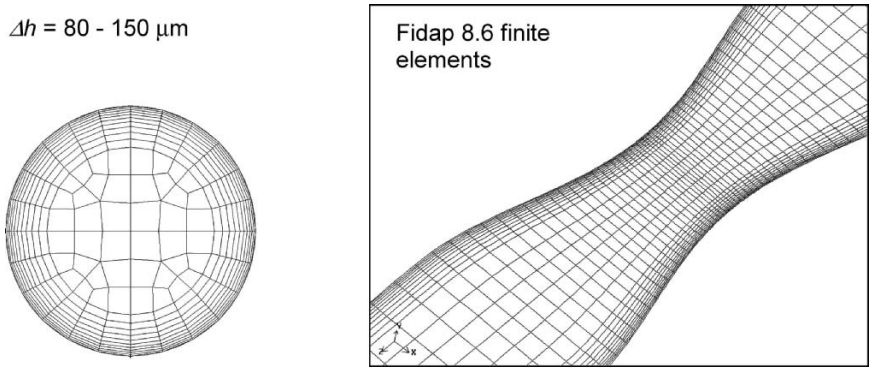

FIGURE 2. Mesh refinement in cross-sectional plane (*left*) and around a stenosis (*right*). The parameter Δh is the dimension of the cell height at the vessel wall.

rate and ν is the kinematic viscosity), the eccentricity or the length of the constriction, many authors noticed that transition to turbulence may appear even at low Reynolds numbers.[1,37] The turbulent two-equation Wilcox model was therefore implemented.[34] This model performs better than the classical standard $\kappa - \varepsilon$ model when flow separation occurs.[11] Through dimensional analysis, the turbulent velocity u_t and vorticity scale δ_t were related to the kinetic energy κ and turbulent frequency ω, respectively by: $u_t \propto \sqrt{\kappa}$ and $\delta_t \propto \sqrt{\kappa}/\omega$. The turbulent dissipation ε was expressed by $\varepsilon = \kappa\omega$, where $54.685 \leq \varepsilon \leq 4373$ mm^2/s^3 and $162 < \kappa < 3600$ mm^2/s^2 depending on the flow rate. The eddy-viscosity was defined according to the Boussinesq constitutive relation.

In the model, the walls were rigid and non-porous and we considered that the fluid was incompressible, Newtonian, and of the same kinematic viscosity as blood, i.e., 3.6×10^{-6} N/m^2. The flow was steady, three-dimensional and turbulent. The usual no-slip velocity specifications were imposed at the walls. At the entrance, a uniform velocity (corresponding to a mean flow rate $Q_m = 250$ ml/min, and to a mean Reynolds number $Re_m = 196$) was set and an entrance length of 10 diameters was thus sufficient to let develop the turbulent velocity profile. At the outlet, traction free conditions were imposed and the velocity was parallel to the longitudinal axis z.

The discretization of the computational domain was achieved with brick finite elements (27 nodes, quadratic interpolation for the velocity and linear interpolation for the pressure). A longitudinal mesh refinement was applied at the stenoses in conjunction with a fine near-wall mesh (see Fig. 2). The use of a segregated algorithm was necessary because of the large number of nodes (300,000–500,000) and thus, of the required storage and computational time. The combination of iterative conjugate gradient solver and preconditioning option was used with mixed velocity-pressure formulation for the solution of the linear equations system. Finally, relaxation and upwinding techniques were used to stabilize the advection terms. The residue and relative error velocity were fixed to 0.001.

Experimental Setup

The experimental test bench (Fig. 3) comprised a pump, a flowmeter, the vascular test section, a distal flow resistance, and a return tank. A peristaltic pump (Micropump, Cole-Parmer Instrument, Vernon Hills, IL) supplied an overflow tank which, by maintaining a constant hydraulic charge, generated a steady flow into the vascular phantom. A piston pump (model 1421, Harvard Apparatus, Holliston, MA) allowed generating pulsatile flows (for two sets of experiments, as listed in Table 1). Three flow regimes were generated in permanent steady flow: $Re_m = 196$, 392, and 588 corresponding respectively, to $Q_m = 250$, 500, and 750 ml/min. These flow rates allowed simulating different potential physiological conditions. The pulsatile flow leaded to a mean Reynolds number of $Re_m = 212$ ($Q_m = 270$ ml/min) and a peak Reynolds of $Re_{max} = 470$ (systolic flow rate of $Q_{max} = 600$ ml/min). Flow rates were recorded from a cannulated probe coupled to an electromagnetic flowmeter (model FM701D,

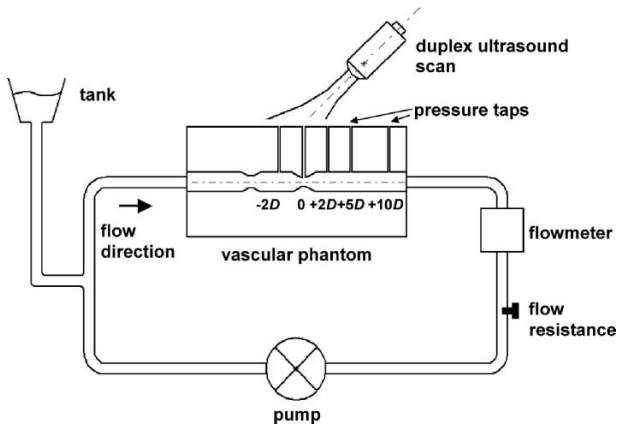

FIGURE 3. Hydrodynamic steady-flow test bench. The pressure taps were localized from $z = -2D$ to $z = +10D$, the origin at $z = 0$ being at the center of the distal stenosis *s2*. The experimental set-up was slightly modified for pulsatile flow experiments.

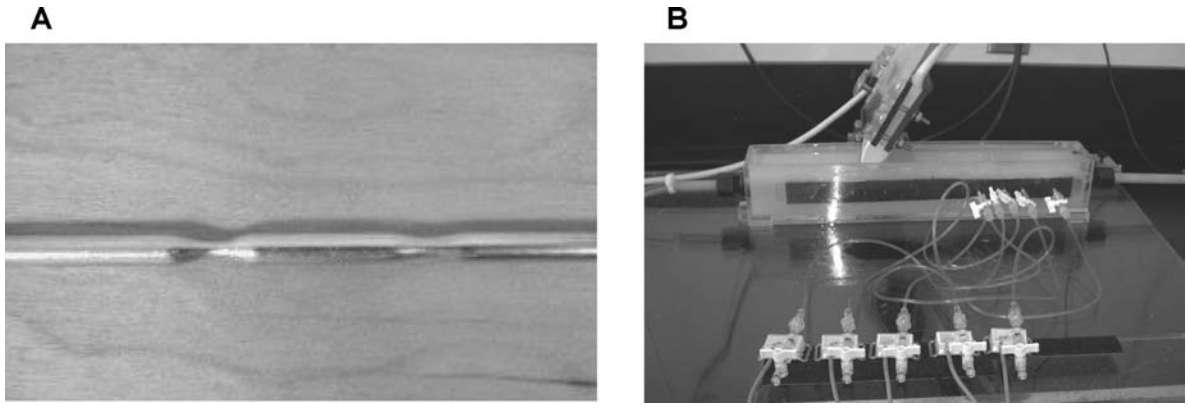

FIGURE 4. Photographs of: (A) the cerrolow rod with a double stenosis (75 and 70% in area reduction) that was fixed into a Plexiglas box and liquefied to produce the vessel lumen; (B) the Plexiglas box filled with agar gel to produce the wall-less vascular phantom following the removal of cerrolow, and pressure taps and echo-Doppler transducer.

Cliniflow II, Carolina Medical, King, NC) and localized at least 20 diameters downstream from the test module. The vascular phantom was enclosed in a Plexiglas container and linked up to the mock flow system by acrylic connectors that did not narrow the tube lumen. Finally, a gate valve acted as a distal resistance to increase static pressure; it was kept constant during each experiment. The blood mimic fluid was a saline mixture of 60%-distilled water and 40%-glycerol. At 20°C, the dynamic viscosity $\mu = \nu/\rho$, where ν is the kinematic viscosity of the fluid and ρ its volumic mass, was 3.5 cP (as measured with a cone-plate viscometer, model LVDVIII-CP-42, Brookfield Engineering Laboratories Inc., Stoughton, MA).

Vascular Phantom Model

As illustrated in Fig. 4, the custom-built test section was constituted of an agar-based wall-less phantom constructed by using a lost-material casting technique with low melting temperature rods made of cerrolow 136 (Cerrometal Products, Bellefonte, PA, USA).[9] The agar solution surrounding the vessel lumen was made of 3.5% agar (Sigma Chemical, St Louis, MO), 8% glycerol (ACP Chemical, Montréal, Canada), and 86% distilled water.[25] Agar gel is known to have similar acoustic properties as living tissues and also to avoid diffraction of the US beam.[9,25] Superfine Sephadex particles (G2550, Sigma Chemical, 1 g/l) acted as US scatterers. B-mode US imaging and histological cuts of a similar vascular phantom were performed to check out if the cross-sectional sections were conformed to what expected. As detailed in Cloutier *et al.*,[9] the geometric accuracy between the diameter of the non-obstructed 7.9-mm diameter rod and that of the sliced lumens measured with a microscope was within −1.4% of the true diameter of the rod. Lastly, each experiment reported in Table 1 (geometric shape and associated hemodynamics) was repeated to enhance the accuracy of the measurements: the wall-less phantoms were replicated three times and measurements were renewed for each mold of the same geometry. The presented results were thus averaged over $n = 3$ experiments.

Pressure and Velocity Measurements

Five pressure taps of 0.83 mm diameter were laid out along the stenotic segment at the following longitudinal positions (referring to the distal stenosis): $-2D$, 0, $+2D$, $+5D$, and $+10D$ (see Fig. 3). A visual B-mode control was made to ensure that needle tips were flush with the internal walls and did not disturb the flow. Finally, pressure taps were connected to disposable medical pressure transducers (Namic Angiographic Systems Division, Glen Falls, NY) and coupled to a 16-channel portable PowerLab monitoring system (ADInstruments, Castle Hill, Australia). A calibration for each tap was performed before each acquisition.

Velocity measurements were performed with an Ultramark HDI-9 system in pulsed-wave Doppler mode. The linear-array transducer (4 MHz) was placed at a pre-set 60° insonification angle as it is usually practiced in clinical Doppler US protocols.[23] The flow phantom was covered by water to ensure adequate coupling with the transducer. The maximum frequency shift (maximum velocity) for steady flow or over the flow cycle for pulsatile flow was read from the displayed Doppler frequency spectrum compensated for the Doppler angle.

RESULTS

The numerical simulations (Figs. 5–7, and 11) allow a detailed description of fluid phenomena. On the other hand, the experimental investigations (Figs. 8–12) are important because they are more closer to clinical conditions and permit the validation of parameters extracted from the numerical models, such as the pressure drop ΔP and the peak systolic velocity ratio PSVR.

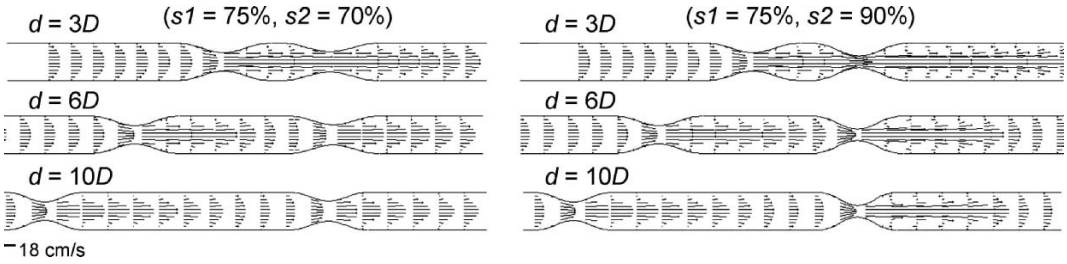

FIGURE 5. Velocity vector fields for different inter-stenotic distances *d* and a Reynolds number $Re_m = 196$ in longitudinal cross-sections.

General Description

For a single stenosis, the flow acceleration at the constriction created a jet bounded by an area of recirculating fluid near the walls. The distance necessary for the downstream maximum velocity to retrieve a velocity similar to the one upstream of the vessel narrowing increased according to the stenosis severity and Reynolds number. In our model of double stenoses, different behaviors were observed depending on the stenosis severity, inter-stenotic distance, and flow conditions. The description given below refers to fluid phenomena observed downstream of *s1* and *s2*, respectively.

If one arbitrarily defines the length of influence *l* of a given stenosis, as the distance necessary for PSVR to retrieve a value inferior to 2, when the upstream velocity RV1 at the entrance of the model is used as the reference velocity, our results showed that *l* beyond *s1* could be longer than the distance between both stenoses *s1* and *s2* (e.g., see Figs. 6(A), 6(B), and 7(B) for an inter-stenotic distance of 3*D*). This demonstrates that two consecutive stenoses may appear as a single long stenosis if PSVR is used as the diagnostic criterion. Furthermore, our results showed that this distance *l* beyond *s1* varied depending on the severity of the distal stenosis *s2*, which proves the hemodynamic interaction between the two stenoses. The influence length of *s1* was shorter than the inter-stenotic distances $d = 6D$ and $d = 10D$.

Now, if one compares a single stenosis *s2* (i.e., the cases in Table 1 for which $d = 0D$) to double stenoses, the influence length *l* beyond *s2* also differed, which also proves the hemodynamic effect of the upstream stenosis *s1* on *s2*. This is shown in Fig. 6, where the influence length beyond *s2* strongly varied depending on the flow rate and double stenosis configuration. Briefly, *l* varied from 1.6*D* for $d = 3D$ to 2.3*D* for $d = 10D$ in the moderate double stenosis model ($s1 = 75\%$, $s2 = 70\%$) for $Re_m = 196$. Conversely, for the same Reynolds number of 196, *l* varied from 5.6*D* for $d = 3D$ to 5.1*D* for $d = 10D$ in the severe double stenosis ($s1 = 75\%$, $s2 = 90\%$). For this specific case, the two stenoses separated by a distance of 3*D* would appear as a long stenosis with an influence length of 5.6*D* beyond *s2* if PSVR ≥ 2 is used as the diagnostic criterion. In our study, the greatest value of *l* beyond *s2* was observed with a short inter-stenotic distance $d = 3D$ and the most severe distal stenosis $s2 = 90\%$.

The PSVR Clinical Index

On Fig. 6, the PSVR index was calculated as $\text{PSVR} = \frac{Vz_i}{\text{RV}}$, where Vz_i is the *z*-component of velocity depicted on the axis of the stenoses at the longitudinal abscissa z_i/D and RV is a reference velocity. In clinical practice, the reference velocity must be taken far from any bifurcation, constriction, or tortuosity.[3] It is usually measured upstream or downstream of the stenosis under evaluation. However, because of collateral branches, clinicians must sometimes measure it inside an atherosclerotic segment, which may impact its significance. The four double stenosis configurations of Fig. 6 show that underestimation of the stenosis severity can be obtained if one uses the reference velocity between both stenoses (RV2) or downstream of *s2* at a distance of 10*D* (RV3). From here on, the results on PSVR were computed with a reference velocity taken upstream at a distance of 10*D* from *s1* (RV1).

Comparison Between Numerical Computations of PSVR and Experiments

As listed in Table 1, data were available to compare the simulations with experiments for inter-stenotic distances $d = 0$, $3D$ and $6D$ at a Reynolds number of 196 for steady flow. Figure 7 presents two examples of double stenosis configurations. As seen, the experimental PSVR values show agreement with the numerical ones. Similar results, not shown here, were obtained for the other configurations.

Influence of the Stenosis Severity, Inter-stenotic Distance, and Reynolds Number on PSVR

To evaluate which parameter was of a greater importance, the maximum PSVR depicted on the central axis at the locations specified in Fig. 3, were plotted according to the flow regime and the inter-stenotic distance. From Fig. 8 (panel A), it can be observed for a single stenosis that PSVR increased with the stenosis severity, whatever the Reynolds

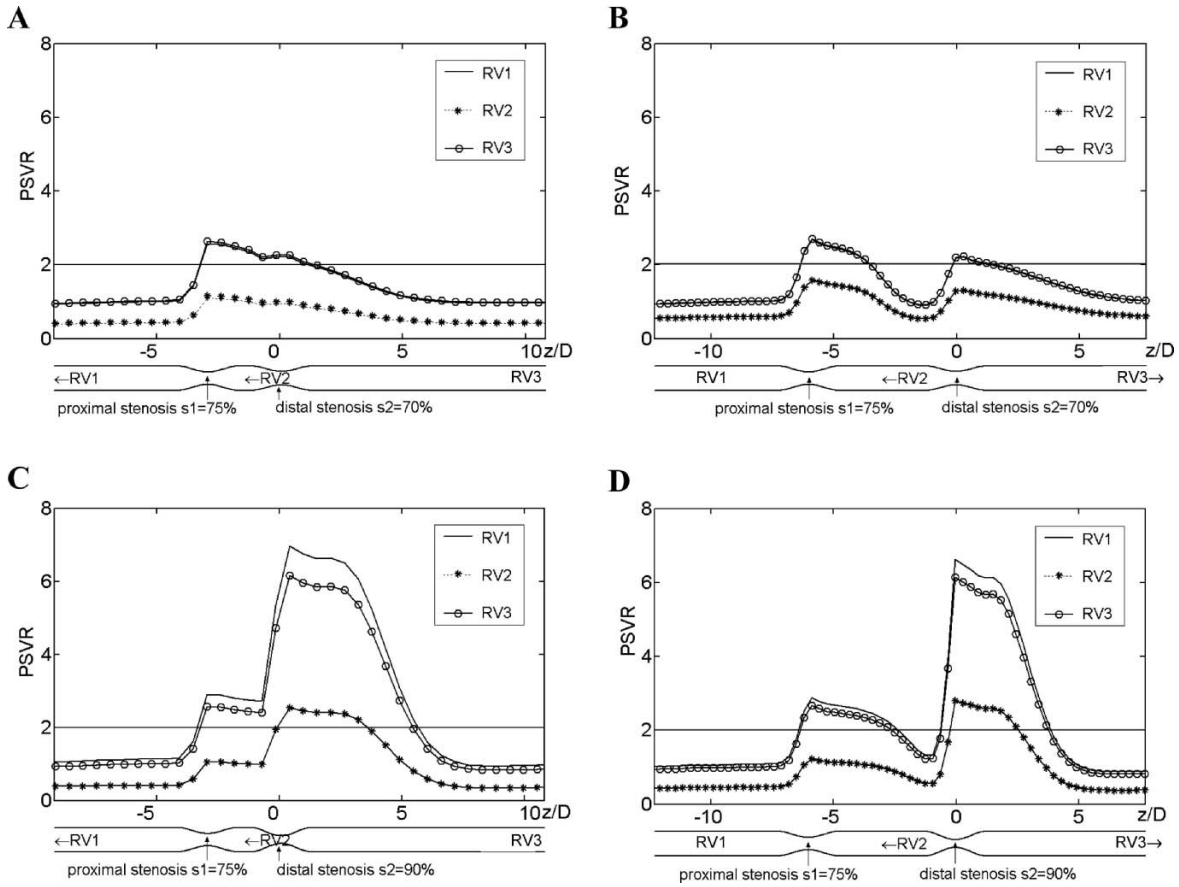

FIGURE 6. Numerical PSVR values along double stenoses under steady flow for a Reynolds number $Re_m = 196$: RV1 corresponds to a reference velocity taken at the entrance (−10*D*), RV2 to a reference velocity measured between both stenoses and RV3 to a reference velocity taken at the outlet (10*D*). (A) $d = 3D$, $s2 = 70\%$; (B) $d = 6D$, $s2 = 70\%$; (C) $d = 3D$, $s2 = 90\%$; (D) $d = 6D$, $s2 = 90\%$. The parameter *d* is the inter-stenotic distance, *D* is the non-obstructed diameter of the vessel, *z* is the longitudinal position along the artery, and PSVR is the ratio of the maximum velocity along the artery to the reference velocity. Note that curves of PSVR measured with the reference velocities RV1 and RV3 are superimposed on panels A and B.

number. For a single stenosis of 70%, the experimental values of PSVR varied from 0.5 to 4.0, whereas for a stenosis of 90%, it was $4.5 \leq \text{PSVR} \leq 8.5$. Intermediate PSVR indices were obtained for the 80% stenosis. The Reynolds number affected PSVR only for the 90% single stenosis. In our models of double stenoses, the presence of a moderate distal stenosis ($s2 = 70\%$ or 80%, see panel B of Fig. 8) had little effects on PSVR, even for a short inter-stenotic distance of 3*D*. PSVR increased for the 75% (*s1*)–90% (*s2*) double stenosis, whatever the Re_m. Surprisingly, elevated flow rates ($Re_m = 392$ and 588 in Fig. 8, panel B) through double stenoses slightly diminished the PSVR index.

On Fig. 9 (panel A), it can be qualitatively observed that an increase of the inter-stenotic distance resulted in a slight reduction of PSVR for a moderate stenosis *s2* of 70%, whatever the Re_m. On the other hand, much higher values of PSVR were observed for a single stenosis of 90% at mean Reynolds numbers of 392 and 588 (Fig. 9, panel B). The inter-stenotic distance between $s1 = 75\%$ and $s2 = 90\%$ had no impact on PSVR for the smallest flow rate considered in this study ($Re_m = 196$).

Effect of Pulsatility on PSVR

When designing this study, the pulsatility of the flow was expected to influence a velocity-related criterion like PSVR. It is shown in Fig. 10 (panel A) that the PSVR maximum was not modified by the unsteadiness of the flow for a moderate stenosis $s2 = 70\%$. On the other hand, inertial effects being strongly increased through a severe constriction of 90% severity (Fig. 10, panel B), the pulsatile PSVR maximum was significantly higher from that obtained in steady flow at $z/D = 2$.

The ΔP Clinical Index

As ΔP is more difficult to determine clinically than PSVR, less attention is devoted here to this index. Under

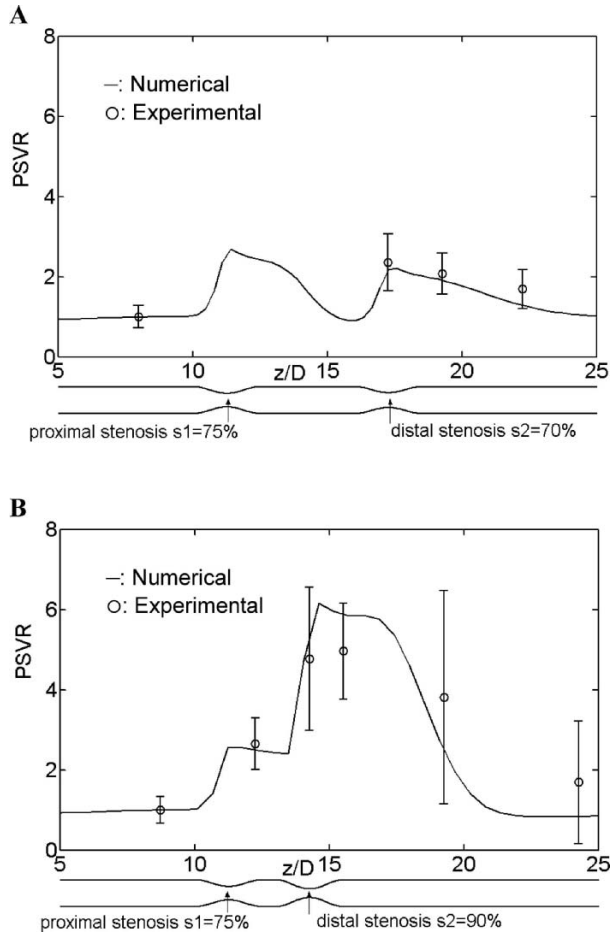

FIGURE 7. Comparison between numerical and experimental PSVR values for double stenoses under steady flow at a Reynolds number $Re_m = 196$: (A) $d = 6D$, $s2 = 70\%$; (B) $d = 3D$, $s2 = 90\%$. The reference velocity RV1 (upstream velocity) was used in the computation of PSVR. See the legend of Fig. 6 for the definition of the other variables.

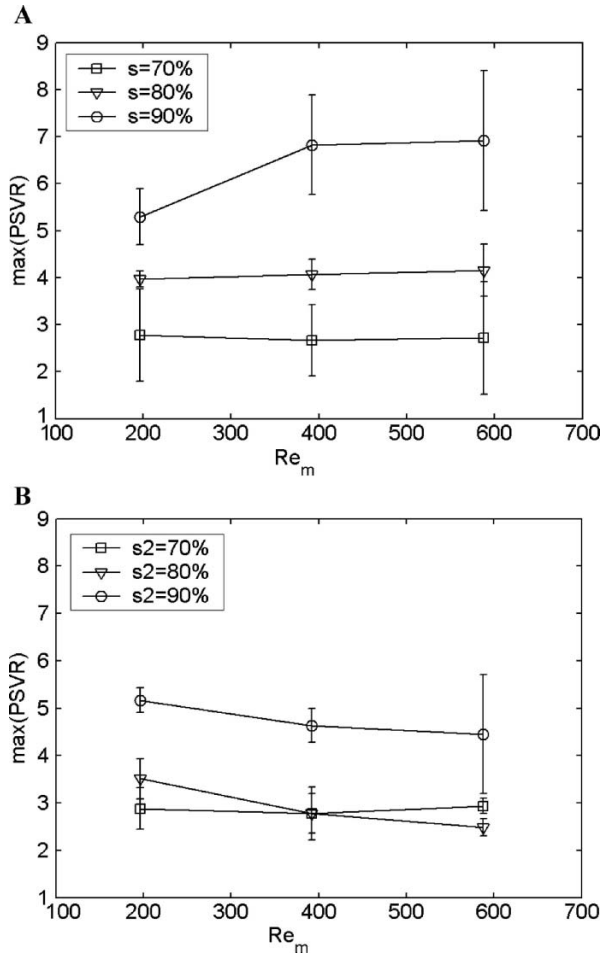

FIGURE 8. Experimental maximum values of PSVR as a function of the Reynolds number Re_m under steady flow for a single stenosis (A) and for a double stenosis configuration with $s1 = 75\%$ and $d = 3D$ (B). The reference velocity RV1 (upstream velocity) was used in the computation of PSVR. See the legend of Fig. 6 for the definition of d and D.

steady flow, the experimental pressure losses (Fig. 11) showed agreement with the numerical simulated ones and allowed the validation of the models. The maximum pressure losses were on the order of 5 mmHg and this was measured within the severe 90% stenosis. The pressure recovery phenomenon observed downstream of stenoses was seen both numerically and experimentally. It was on the order of a few millimeter of mercury depending on the stenosis severity. It is also shown in Fig. 11 (panel B) that the pressure losses were not notably changed by the unsteadiness of the flow.

DISCUSSION

The Doppler US clinical index PSVR ≥ 2 is generally accepted to identify stenosis severity greater than 75%, but this index does not perform well for detecting the length of a single constriction or the presence of multiple lesions. Thus, in this study, we attempted to describe the PSVR evolution in conjunction with single/double stenoses of known geometries.

From numerical studies, it was shown that PSVR is intrinsically linked to the complex velocity field upstream and downstream of the stenoses. Tracking its maximum value along an artery is equivalent of determining the location of the most severe stenosis. In contrast, its longitudinal evolution poorly reflects the length of the lesion or the impact of surrounding stenoses (if a threshold of 2 is used to define the length of influence of the jet l, which is usually the decision criterion for identifying the presence of a critical stenosis $>75\%$). As proposed by Leng *et al.*,[18] a cut-off value of PSVR $= 2$ is highly sensitive whereas a value of 3 gives a high specificity. The prospective and multicentric study of Idu *et al.* [13] showed that PSVR > 3 gave an optimal

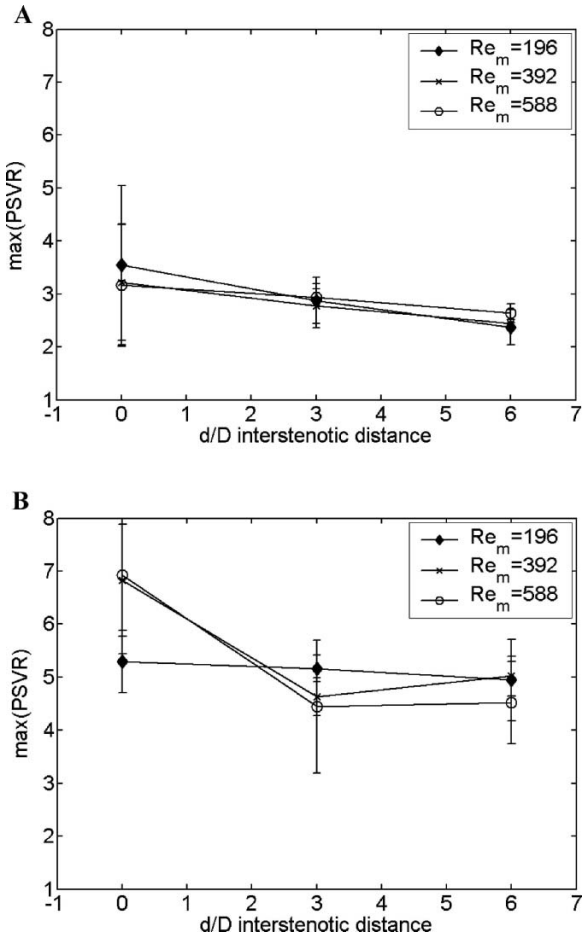

FIGURE 9. Experimental maximum values of PSVR as a function of the inter-stenotic distance *d* / *D* under steady flow for *s2* = 70% (A) and *s2* = 90% (B) for different Reynolds number Re_m. The reference velocity RV1 (upstream velocity) was used in the computation of PSVR. The parameter *d*/*D* = 0 corresponds to the case of a single stenosis. See the legend of Fig. 6 for the definition of *d* and *D*.

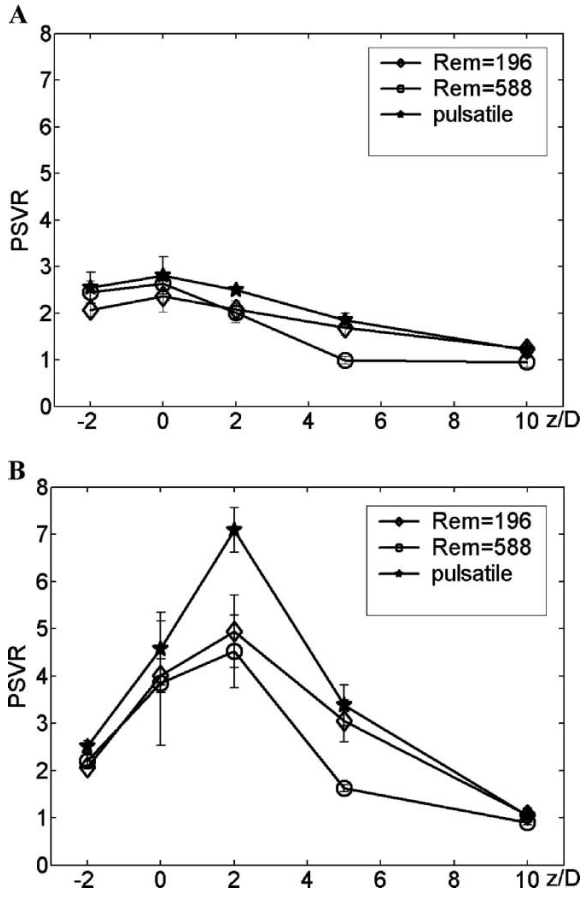

FIGURE 10. Experimental evolution of PSVR values along the longitudinal axis of the vessel *z* for Reynolds numbers Re_m = 196 and 588 (steady flow) and for Re_m = 212 (pulsatile flow): *s2* = 70% (A), *s2* = 90% (B). The reference velocity RV1 (upstream velocity) was used in the computation of PSVR. The parameter *d*/*D* = 0 corresponds to the case of a single stenosis. For double stenoses, *s1* = 75%. See the legend of Fig. 6 for the definition of *d* and *D*.

sensitivity (Se) of 80% and a specificity (Sp) of 84% to predict the presence of a 90% lesion. In De Smet *et al.*,[10] isolated (single) stenoses graded by angiography resulted in the following PSVR threshold values: PSVR $\geq$ 2.8 for $s_{\%} \geq$ 75% (Se = 86%, Sp = 84%), and PSVR $\geq$ 5 for s% $\geq$ 94% (Se = 65%, Sp = 91%). A French study[19] proposed a PSVR cut-off value of 2.5 below which stenoses are expected to be of a moderate severity ($s_{\%} < 75\%$).

The reliability of PSVR in the presence of multiple lesions has been subject to clinical controversy. Some authors[8,26] reported that the performance of Doppler US *in vivo* was linked to the existence of adjacent lesions. Sacks *et al.*[26] chose a lower critical PSVR of 1.4 for the detection of lesions. They also noticed a poor sensitivity for the detection of a second stenosis but a good specificity. In contrast, Sensier *et al.*[28] concluded that PSVR $\geq$ 2 was efficient to detect isolated lesions (even if the sensitivity was low: Se = 65%, Sp = 96%) as well as adjacent lesions (Se = 88%, Sp = 86%). Indeed, Aly *et al.*[5] proved that PSVR > 2 was less sensitive in the presence of isolated lesions when compared to multiple stenoses.

These controversial findings demonstrate that the major difficulty is to find the best compromise in the choice of the PSVR threshold. It is clear from our study (see Fig. 6) that it is difficult to distinguish stenoses separated by a distance of 3*D* with this criterion because PSVR does not return to a value below 2 between both lesions. If one assumes that the position and severity of each stenosis is known (e.g., if a gold standard examination such as 3D angiography was available), choosing this cut-off of PSVR > 2 with our data would have resulted in detecting almost all stenoses (77/78) whose severity was over 70%. Based on this finding, it would be possible to say that multiple stenoses do not affect

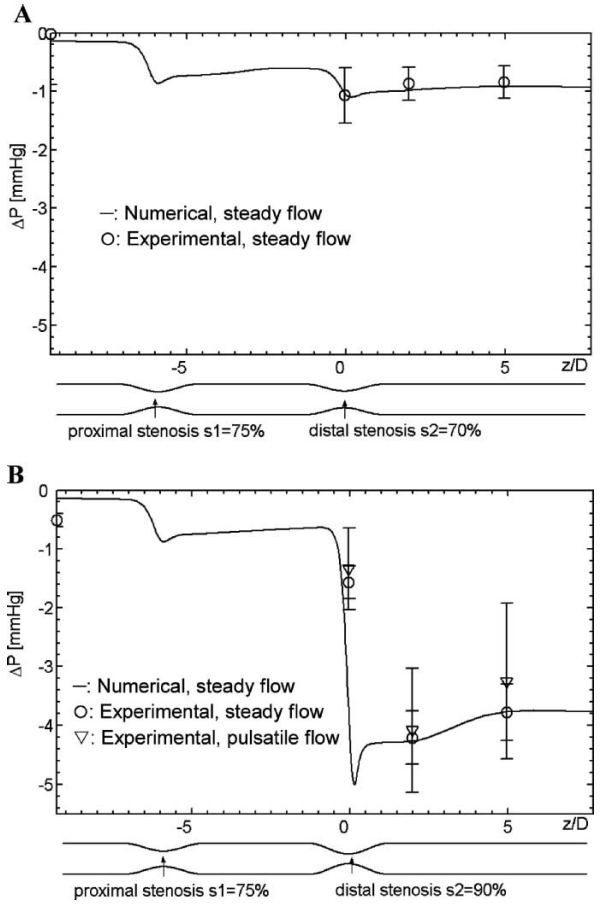

FIGURE 11. Comparison between numerical and experimental pressure losses ΔP for double stenoses at a Reynolds number $Re_m = 196$ in steady flow and $Re_m = 212$ in pulsatile flow: (A) $d = 6D$, $s2 = 70\%$; (B) $d = 6D$, $s2 = 90\%$. See the legend of Fig. 6 for the definition of z, d and D. In panel A, the maximum numerical and experimental pressure losses along the model were 1.10 mmHg and 0.93 mmHg, respectively. In (B) they were 5.00 mmHg and 4.35 mmHg, respectively.

the detection of moderate-to-severe stenoses >70%. However, if one considers that specific lesions may be missed and misinterpreted as a single long stenosis, we must conclude that multiple stenoses affect the clinical decision making. Figures 7–9 also suggest that PSVR > 4 could allow detecting a severe stenosis of 90% but with a sensitivity and specificity not reaching 100%. Indeed, the flow condition (Fig. 8) and the inter-stenotic distance (Fig. 9) can result in a range of PSVR values above or below that threshold in the presence of multiple stenoses.

Interpretation of the Results

As noted in panel B of Fig. 8, elevated flow rates (Re_m = 392 and 588) through double stenoses under steady flow slightly diminished the PSVR index in the experiments. Those results appeared surprising since the velocity downstream of *s2*, and consequently PSVR, would have been expected to be higher as the flow rate was increased. These particular flow phenomena could be induced by vortex shedding and turbulence occurring in steady flow, as well as in pulsatile flow, downstream of *s2*. Oscillations of the central velocity may have also occurred experimentally and as a consequence, if the US velocity measurements happened not to be performed continuously along the artery, the real maximum velocity could have been missed, which can also explain our results (see[29]).

Reproducibility—Limitations of the Study

Through this study, experimental variabilities of PSVR have been observed, even for the same geometrical configurations. Limitations of the US technique have already been established.[15] With conventional Doppler US, Hoskins[12] reported that errors, associated with geometric spectral broadening and measurement of the true beam-vector angle, could induce a significant variation of up to 35% when estimating the maximum velocity. In clinical practice, disparity between US settings (like the wall filter or gain[12,30]) makes the PSVR to vary from one patient to another for the same stenosis severity and similar hemodynamic conditions.[31] Nevertheless, because all measurements reported in this study were performed under controlled conditions (flow rate, Doppler angle, flow geometry, etc . . .), our study suggests that the variability of PSVR was mainly due to the nature of the flow, which depends strongly on the stenosis morphology (severity, shape, length,[27] axisymmetry of the constriction[21]). These typical jet flows are intrinsically unstable and even a slight imperfection in the straightness of the tube can lead to strong three-dimensional effects. Cross-sectional images in Doppler color-mode highlighted asymmetric zones of recirculating fluid (see Fig. 12). As seen on this figure, successive deflections of the post-stenotic jet were encountered downstream of some stenoses. These experimental observations of flow instability are in agreement with those of Seeley and Young.[27]

The limitations in the use of the PSVR index can be highlighted in laboratory experiences where optimal conditions are put together. One can easily imagine that other difficulties may reach out in clinical protocols. The general behavior of double stenoses cannot easily be defined because of the strong dependence upon geometric parameters (distance between stenoses, severity and length of the lesion), each idealized single/multiple stenoses induce specific hemodynamic patterns, which varies with the flow regime and the inlet flow waveform. So this work, puts into the clinical context, suggests that it is not surprising to read contradicting conclusions in the literature concerning the impact or not of multiple stenoses on Doppler US derived indices used to diagnose lower limb vascular diseases.

Finally, it is to note that the assumptions supporting the 3D turbulent flow modeling (i.e., rigid arterial wall and axi-symmetric vessel) corroborated the experimental conditions of the phantom study. For instance, the axi-symmetric

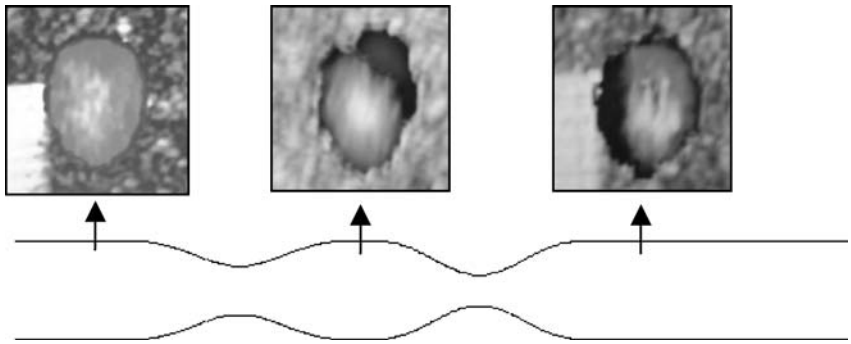

FIGURE 12. Successive deflections of the post-stenotic jet in cross-sectional planes under steady flow (color Doppler mode) for a Reynolds number $Re_m = 196$, an inter-stenotic distance $d = 3D$, a proximal stenosis $s1 = 75\%$, and a distal stenosis $s2 = 90\%$ in area reduction. See the legend of Fig. 6 for the definitions of the parameters d and D.

vessel phantom had non-compliant vessel wall made of agar gel confined in a Plexiglas box. If one undertakes simulations of realistic human arterial geometries including fluid-structure interactions to consider the pulsatility of the wall, other conclusions may result. However, it is believed that the hemodynamic interactions between multiple stenoses will remain and even be amplified.

CONCLUSIONS

Our study showed agreements between the pressure loss (ΔP) and the peak systolic velocity ratio (PSVR) extracted from the steady flow numerical computations and experiments. This suggests that flow modeling in realistic vessel geometries may become of value to predict hemodynamic features that are difficult to measure in a patient (e.g., ΔP across stenoses). The modeling of turbulent flow in double stenosis configurations constituted a technical challenge of the present study because of the computer data storage needed, the extensive computational time cost and the mesh refinement requirement, especially at the wall. It is worth mentioning that computational fluid dynamic modeling of physiologically turbulent flow is still in its relative infancy.[33]

The current study also showed that the total influence length of a stenotic jet differed if one considers a single stenosis or a double stenosis configuration. This length beyond the proximal stenosis *s1* of 75% area reduction was longer than the distance between both stenoses for the case of the inter-stenotic distance of 3-vessel diameters, at all Reynolds numbers tested. Thus, our study showed that two consecutive stenoses may appear as a single long stenosis if PSVR is used as the clinical diagnostic criterion. We also demonstrated that the proximal stenosis *s1* modified the influence distance beyond the distal stenosis *s2* that was varied between 70 and 90% area reductions. Both results proved the mutual hemodynamic interaction between both stenoses *s1* and *s2*.

According to the steady flow simulations and experimental results in both steady and pulsatile flows, tracking the maximum value of PSVR along an artery was shown to be equivalent of determining approximately the location of the most severe stenosis. For two moderate stenoses ($s1 = 75\%$ and $s2 = 70\%$ area reductions), the maximum of PSVR along the vessel did not differ from the case of a single moderate stenosis of 70%, whatever the flow rate. For the most severe double stenosis configuration ($s1 = 75\%$ and $s2 = 90\%$ area reductions), the maximum of PSVR was reduced compared to the case of a single stenosis of 70% at the highest flow rates. These conclusions may be used as guidelines for clinical scans. However, one should consider these findings with caution. For instance, since it was shown that the instability of the jet increased the variability of our experimental results, ever larger variability may be expected for *in vivo* scans in complex 3D vessel geometries. Future work should thus focus on flow experiments and modeling in realistic diseased vessels.

ACKNOWLEDGMENTS

This work was supported by a merit fellowship for post-doctoral research of the Quebec Ministry of Education (to C.B.), a studentship from the Natural Sciences and Engineering Research Council of Canada (to. B.L.), and a grant from the Canadian Institutes of Health Research (#MOP-53244 to G.C., L.G.D., G.S.). Drs. Soulez and Cloutier are respectively recipient of a clinical research scholarship award and of a national scientist award from the Fonds de la Recherche en Santé du Québec. Dr. Bertolotti performed this work at the Institut de Recherches Cliniques of Montreal, and then with the Équipe Biomécanique Cardiovasculaire, EGIM, at the C.N.R.S. (I.R.P.H.E.) UMR 6594, Marseille, France. The authors acknowledge Philips Medical System (Dr. Helen Routh) for the loan of the ultrasound system used in this study.

REFERENCES

[1]Ahmed, S. A., and D. P. Giddens. Pulsatile flow studies with laser Doppler anemometry. *J. Biomech.* 17:695–705, 1984.

[2]Allard, L., G. Cloutier, L. G. Durand, *et al*. Limitations of ultrasonic duplex scanning for diagnosing lower limb arterial stenoses in the presence of adjacent segment disease. *J. Vasc. Surg*. 19(4):650–657, 1994.

[3]Allard, L., G. Cloutier, and L. G. Durand. Doppler velocity ratio measurements evaluated in a phantom model of multiple arterial disease. *Ultrasound Med. Biol*. 21(4):471–480, 1995.

[4]Allard, L., G. Cloutier, Z. Guo, *et al*. Review of the assessment of single level and multilevel arterial occlusive disease in lower limbs by duplex ultrasound. *Ultrasound Med. Biol*. 25(4):495–502, 1999.

[5]Aly, S., M. P. Jenkins, F. H. Zaidi, *et al*. Duplex scanning and effect of multisegmental arterial disease on its accuracy in lower limb arteries. *Eur. J. Vasc. Endovasc. Surg*. 16:345–349, 1998.

[6]Ang, K. C., and J. Mazumdar. Mathematical modelling of triple arterial stenoses. *Australas. Phys. Eng. Sci. Med*. 18(2):89–94, 1995.

[7]Back, M. R., A. N. Bowser, D. C. Schmacht, *et al*. Duplex selection facilitates single point-of-service endovascular and surgical management of aortoiliac occlusive disease. *Ann. Vasc. Surg*. 16(5):566–574, 2002.

[8]Bergamini, T. M., C. M. Tatum Jr, C. Marshall, *et al*. Effect of multilevel sequential stenosis on lower extremity arterial duplex scanning. *Am. J. Surg*. 169(6):564–566, 1995.

[9]Cloutier, G., G. Soulez, S. D. Qanadli, *et al*. A multimodality vascular imaging phantom with fiducial markers visible in DSA, CTA, MRA and ultrasound. *Med. Phys*. 31(6):1424–1433, 2004.

[10]De Smet, A. A., E. J. Ermers, and P. J. Kitslaar. Duplex velocity characteristics of aortoiliac stenoses. *J. Vasc. Surg*. 23(4):628–636, 1996.

[11]Ghalichi, F., X. Deng, A. De Champlain, *et al*. Low Reynolds number turbulence modeling of blood flow in arterial stenoses. *Biorheology* 35:281–294, 1998.

[12]Hoskins, P. R.. A comparison of single- and dual-beam methods for maximum velocity estimation. *Ultrasound Med. Biol*. 4:583–592, 1999.

[13]Idu, M. M., J. D. Blankenstein, P. De Gier, *et al*. Impact of color-flow duplex surveillance program on infrainguinal vein graft patency: A five-year experience. *J. Vasc. Surg*. 17:42–52, 1993.

[14]Jager, K. A., D. J. Phillips, R. L. Martin, *et al*. Noninvasive mapping of lower limb arterial lesions. *Ultrasound Med. Biol*. 11(3):515–521, 1985.

[15]Jones, S.A.. Fundamental sources of error and spectral broadening in Doppler ultrasound signals. *Crit. Rev. Biomed. Eng*. 21(5):399–483, 1993.

[16]Latornell, D. J., A. Pollard. Some observations on the evolution of shear layer instabilities in laminar flow through axisymmetric sudden expansion. *Phys. Fluids* 29(9):677–681, 1986.

[17]Lee, T. S. Steady laminar fluid flow through variable constrictions in vascular tube. *J. Fluids Eng*. 116:66–71, 1994.

[18]Leng, G. C., M. R. Whyman, P. T. Donnan, *et al*. Accuracy and reproducibility of duplex ultrasonography in grading femoropopliteal stenoses. *J. Vasc. Surg*. 17(3):510–517, 1993.

[19]Matignon, Y. Échographie-Doppler dans l'artériopathie oblitérante des membres inférieurs. *©Agence Nationale d'Accréditation et d'Évaluation en Santé*. Juin 2002. Available at: http://www.anaes.fr/anaes/Publications.nsf/nPDFFile/RA_LILF-5EHJD7/$File/echodoppler.rap.pdf. Accessed on October, 2003.

[20]Moneta, G. L., R. A. Yeager, R. Antonovic, *et al*. Accuracy of lower extremity arterial duplex mapping. *J. Vasc. Surg*. 15(2):275–284, 1992.

[21]Ojha, M., R. S. C. Cobbold, K. W. Johnston, *et al*. Pulsatile flow through constricted tube: An experimental investigation using photochromic methods. *J. Fluid Mech*. 203:173–197, 1989.

[22]Pincombe, B., J. Mazumdar, I. Hamilton-Craig. Effects of multiple stenoses and post-stenotic dilatation on non-Newtonian blood flow in small arteries. *Med. Biol. Eng. Comput*. 37(5):595–599, 1999.

[23]Ramaswami, G., A. Al-Kutoubi, A. N. Nicolaides, *et al*. The role of duplex scanning in the diagnosis of lower limb arterial disease. *Ann. Vasc. Surg*. 13(5):494–500, 1999.

[24]Ranke, C., A. Creutzig, and K. Alexander. Duplex scanning of the peripheral arteries: correlation of the peak velocity ratio with angiographic diameter reduction. *Ultrasound Med. Biol*. 18(5):433–440, 1992.

[25]Rickey, D. W., P. A. Picot, D. A. Christopher, *et al*. A wallless vessel phantom for Doppler ultrasound studies. *Ultrasound Med. Biol*. 21(9):1163–1176, 1995.

[26]Sacks, D., M. L. Robinson, D. L. Marinelli, *et al*. Peripheral arterial Doppler ultrasonography: diagnostic criteria. *J. Ultrasound Med*. 11(3):95–103, 1992.

[27]Seeley, B. D., and D. F. Young. Effect of geometry on pressure losses across models of arterial stenoses. *J. Biomech*. 9:439–448, 1976.

[28]Sensier, Y., T. Hartshorne, A. Thrush, *et al*. The effect of adjacent segment disease on the accuracy of colour duplex scanning for the diagnosis of lower limb arterial disease. *Eur. J. Vasc. Endovasc. Surg*. 12(2):238–242, 1996.

[29]Siouffi, M., V. Deplano, and R. Pélissier. Experimental analysis of unsteady flows through a stenosis. *J. Biomech*. 31(1):11–19, 1997.

[30]Steinman, A. H., J. Tavakkoli, J. G. Myers, *et al*. Sources of errors in maximum velocity estimation using linear-array doppler systems with steady flow. *Ultrasound Med. Biol*. 5:655–664, 2001.

[31]Ubbink, D. T., M. Fidler, and D. A. Legemate. Interobserver variability in aortoiliac and femoropopliteal duplex scanning. *J. Vasc. Surg*. 33:540–545, 2001.

[32]van Dreumel, S. C., and G. D. C. Kuiken. Steady flow through a double converging-diverging tube model for mild stenoses. *J. Biomech. Eng*. 111:212–221, 1989.

[33]Varghese, S. S., and S. H. Frankel. Numerical modeling of pulsatile turbulent flow in stenotic vessels. *J. Biomech. Eng*. 125:445–460, 2003.

[34]Wilcox, D. C. *Turbulence Modeling for CFD*. DCW Industries Inc., 1993.

[35]Young, D., and F. Tsai. Flow characteristics in models of arterial stenoses—II. Unsteady flow. *J. Biomech*. 6:547–559 1973.

[36]Young, D., N. Cholvin, R. Kirkeeide, and A. Roth. Hemodynamics of arterial stenoses at elevated flow rates. *Circ. Res*. 41(1):99–107, 1977.

[37]Youngchareon, W., and D. Young. Initiation of turbulence in models of arterial stenoses. *J. Biomech*. 12:185–196, 1979.